faces and at other locations inside the specimens while the top face temperature was controlled according to a preselected program. This experimental program is described in detail in Ref. 2.

Comparison of experimental and predicted results

Measured skin temperatures, rather than heat flux, were used as inputs to the computer program to predict thermal response. A typical comparison of experimental and predicted results is shown in Fig. 3. The agreement between measured and predicted midcell temperature is excellent. The poor agreement between measured and predicted top braze temperature is probably a result of faulty braze, hence imperfect contact between the top face and the core wall near the location of the thermocouple used to measure braze temperature. Post test inspection revealed faulty or damaged braze on several panels. For the large cell panels described in Table 1, excellent agreement was obtained between measured and predicted temperature at the top braze.

Good general agreement between experimental and predicted results serves to recommend the analysis for use in design studies.

References

[1] Kendall, P. J., "Thermal response in sandwich panels," Martin Orlando Rept. OR 6037, Flight Dynamics Lab. FDL-TDR-64-135 (October 1964).

[2] Kendall, P. J., Moran, J. P., and Chappell, T. E., "A method for predicting thermal response in sandwich panels," Martin Orlando Rept. OR 2996 Aeronautical Systems Div. ASD-TDR-63-306 (May 1963).

[3] Eckert, E. R. G., *Heat and Mass Transfer* (McGraw-Hill Book Co., Inc., New York, 1959).

[4] Dusinberre, G. M., *Heat Transfer Calculations by Finite Differences* (International Textbook Co., Scranton, Pa., 1961).

[5] Malcolm, J. R. and Slack, R. L., "Comparison of relative costs of thermal analysis methods for hypersonic vehicle compartments," Wright Air Development Div. WADD TR 60-768 (July 1961).

Examination of an Aerodynamic Coupling Phenomenon

RICHARD F. PORTER* AND JAMES P. LOOMIS*
Battelle Memorial Institute, Columbus, Ohio

Nomenclature

b = wing span, ft
$\bar{c}$ = mean aerodynamic chord, ft
c.g. = center of gravity
C_l = rolling moment coefficient†
C_L = lift coefficient†
C_m = pitching moment coefficient†
C_n = yawing moment coefficient†
g = gravitational constant, ft/sec^2
h = pressure altitude, ft
I_x = roll axis moment of inertia, slug·ft^2
I_y = pitch axis moment of inertia, slug·ft^2
I_z = yaw axis moment of inertia, slug·ft^2
L_α = $\rho S b V_0^2 \beta_0 C_{l_{\beta_\alpha}}/2I_x$, 1/sec^2
L_β = $\rho S b V_0^2 C_{l\beta}/2I_x$, 1/sec^2
L_p = $\rho S b^2 V_0 C_{l_p}/4I_x$, 1/sec
L_r = $\rho S b^2 V_0 C_{l_r}/4I_x$, 1/sec
m = aircraft mass, slugs
M = Mach number
MAC = mean aerodynamic chord
M_α = $\rho S \bar{c} V_0^2 C_{m_\alpha}/2I_y$, 1/sec^2
M_β = $\rho S \bar{c} V_0^2 C_{m\beta}/2I_y$, 1/sec^2
M_q = $\rho S \bar{c}^2 V_0 C_{m_q}/4I_y$, 1/sec
N_α = $\rho S b V_0^2 \beta_0 C_{n_{\beta_\alpha}}/2I_z$, 1/sec^2
N_β = $\rho S b V_0^2 C_{n\beta}/2I_z$, 1/sec^2
N_p = $\rho S b^2 V_0 C_{n_p}/4I_z$, 1/sec
N_r = $\rho S b^2 V_0 C_{n_r}/4I_z$, 1/sec
p = rolling rate, rad/sec
q = pitching rate, rad/sec
r = yawing rate, rad/sec
S = wing area, ft^2
T = total engine thrust, lb
V_0 = equilibrium true airspeed, fps
Y_β = $-(T \cos\beta_0/mV_0) + (\rho S V_0 C_{y\beta}/2m)$, 1/sec
Z_α = $-(T \cos\alpha_0/mV_0 \cos\beta_0) - (\rho S V_0 C_{L_\alpha}/2m \cos\beta_0)$, 1/sec
α = angle of attack, rad
β = sideslip angle, rad
Δ_{lat} = determinant of the lateral-directional equation's coefficient matrix, 1/sec^4
Δ_{long} = determinant of the longitudinal equation's coefficient matrix, 1/sec^2
λ = differential operator, 1/sec
ρ = atmospheric density, slug/ft^3
ϕ = bank angle, rad

Received August 16, 1965.

* Senior Aeronautical Research Engineer, Columbus Laboratories. Member AIAA.

† Note: Subscripts to these coefficients represent the partial derivative of the coefficients with respect to the subscript variable. Where such subscripts are the angular rates p, q, or r, the derivatives are actually with respect to the conventional nondimensionalized forms of the rates [i.e., $C_{l_p} = \partial C_l/\partial(pb/2V_0)$].

Introduction

AN interesting form of coupling between the longitudinal and lateral-directional rigid body modes of aircraft trimmed at nonzero sideslip angles has been observed and analyzed by the authors. The observed effect of this coupling is a degradation of the dutch roll damping compared to that at zero sideslip trim.

The phenomenon was observed during analog simulation studies of swept-wing transport operations in turbulence, during which the simulated aircraft was flown at exaggerated nonzero sideslip trim conditions. In none of the observed cases did the rate of divergence nor frequency of the motion pose serious control difficulties; in addition, the equilibrium sideslip angles required for pronounced coupling effects were well beyond those that may reasonably be expected for this class of aircraft. Nevertheless, a brief analysis‡ was performed to identify the mechanism of the coupling and to suggest avenues for further research.

Analysis

For this analysis, a set of linearized equations were derived with 5 degrees-of-freedom. Only velocity was assumed constant, thereby retaining all rigid body modes except the phugoid. These linearized equations were derived in the usual manner by restricting the motion to infinitesimal disturbances, or perturbations, from a reference equilibrium state.[1]

A novel feature of the equations developed here is that the chosen equilibrium condition is one with a finite value of sideslip, the wings being held level by appropriate lateral control, necessitating a small equilibrium yawing velocity to provide a quasi-static balance. The equilibrium sideslip could have been balanced by an appropriate bank angle with zero yaw rate, or any proper combination thereof, but the former choice promoted certain computational simplifications. In any event, it is not felt that the exact choice of equilibrium state significantly modifies the ensuing aircraft dynamic characteristics as long as the essential feature, an equilibrium sideslip angle, is permitted. The equations were derived using a principal body axes system for the rotational degrees-of-freedom, and a special wind axes system for the two translational equations.

As the derivation progressed, many terms appeared which serve to couple the longitudinal and the lateral-directional

‡ This was supported by a research grant from Northwest Airlines, Inc.

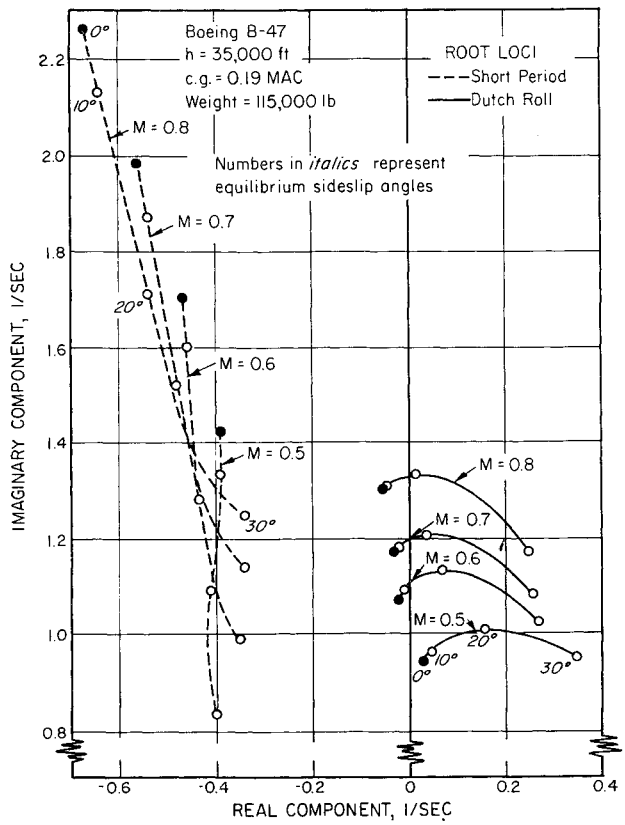

Fig. 1 Variation of short period and dutch roll roots with equilibrium sideslip angle, at a c.g. position of 0.19 MAC and various Mach numbers.

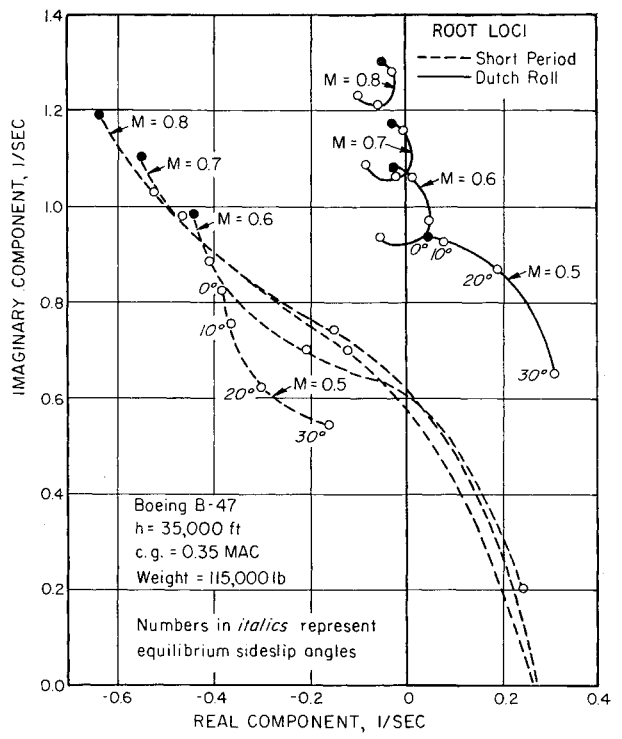

Fig. 2 Variation of short period and dutch roll roots with equilibrium sideslip angle, at a c.g. position of 0.35 MAC and various Mach numbers.

equations. To be specific, the kinematic term in the angle-of-attack equation indicates a roll rate influence as a first-order effect if an equilibrium sideslip angle exists. In addition, several of the lateral-directional aerodynamic coefficients are strongly dependent upon angle of attack. In some cases, the inclusion of an equilibrium sideslip angle introduces new stability derivatives that are nonexistent in the classical zero-sideslip linearized equations.

To illustrate how these new stability derivatives occur as a consequence of our assumed equilibrium state, consider the rolling moment coefficient C_l. Assume that C_l is a function of angle of attack, sideslip angle, roll rate, and yaw rate.

Expanding C_l by Taylor's series and retaining all first-order terms yields

$$C_l = (C_l)_0 + (\partial C_l/\partial\alpha)_0 (\alpha - \alpha_0) + (\partial C_l/\partial\beta)_0 (\beta - \beta_0) + (\partial C_l/\partial p)_0 (p - p_0) + (\partial C_l/\partial r)_0 (r - r_0) \quad (1)$$

If the variables in Eq. (1) are now considered to represent the change from the reference state, and if conventional stability derivative notation is used, we obtain

$$C_l = C_{l_\alpha}\cdot\alpha + C_{l_\beta}\cdot\beta + C_{l_p}\cdot p + C_{l_r}\cdot r \quad (2)$$

Now, all of these stability derivatives must be evaluated at the equilibrium condition. Furthermore, if C_l is a linear function of sideslip for a fixed angle of attack, then,

$$C_{l_\alpha} = (\partial C_{l_\beta}/\partial\alpha)_0\, \beta_0 \quad (3)$$

A new stability derivative is thus obtained and Eq. (2) becomes

$$C_l = (\beta_0 C_{l_{\beta_\alpha}})\alpha + C_{l_\beta}\cdot\beta + C_{l_p}\cdot p + C_{l_r}\cdot r \quad (4)$$

This technique was also employed with the yawing moment coefficient to derive the first-order angle-of-attack effects.

The five dynamic equations together with a kinematic constraint equation for the bank angle geometry comprise a set of six simultaneous linear homogeneous equations. These equations appear in operational form as Eq. (5):

$$\begin{bmatrix} (Z_\alpha - \lambda) & 1 & 0 & -(\tan\beta_0 \cos\alpha_0) & -(\tan\beta_0 \sin\alpha_0) & 0 \\ M_\alpha & (Mq - \lambda) & M_\beta & 0 & 0 & 0 \\ 0 & 0 & (Y_\beta - \lambda) & \sin\alpha_0 & -\cos\alpha_0 & (g/V_0) \\ L_\alpha & 0 & L_\beta & (L_p - \lambda) & L_r & 0 \\ N_\alpha & 0 & N_\beta & N_p & (N_r - \lambda) & 0 \\ -(\lambda \sin\beta_0) & (\sin\beta_0) & 0 & (\cos\beta_0 \cos\alpha_0) & (\cos\beta_0 \sin\alpha_0) & -\lambda \end{bmatrix} \cdot \begin{bmatrix} \alpha \\ q \\ \beta \\ p \\ r \\ \phi \end{bmatrix} = \begin{bmatrix} 0 \\ 0 \\ 0 \\ 0 \\ 0 \\ 0 \end{bmatrix} \quad (5)$$

The determinant of the coefficient matrix, upon expansion, yields a sixth degree polynomial in λ. Setting this polynomial equal to zero provides the characteristic equation of the system. In this analysis, a digital computer program was employed to solve for the roots of the characteristic equation using the equilibrium sideslip angle as a parameter for each flight condition.

In the experimental phase of the analysis, the characteristics of the B-47 aircraft were examined extensively at several flight conditions and equilibrium sideslip angles. Pertinent data, including static aeroelastic effects, were obtained from Ref. 2. This exercise revealed that there are substantial changes in the period and damping of the short-period and dutch roll modes as the equilibrium sideslip angle is varied. Figures 1–3 illustrate some of the results. As shown in Fig. 1, at the forward c.g. positions, increased equilibrium sideslip causes the dutch roll mode to tend toward instability. However, Fig. 2 shows that at the aft c.g. positions, it is the short-period mode that is destabilized under the increased equilibrium sideslip. Finally, Fig. 3 shows the root loci for a series

of c.g. positions at Mach 0.6. In this case, a c.g. position between 0.30 MAC and 0.32 MAC appears to be the point at which either dutch roll or short-period becomes destabilized.

To identify the physical source of the motion depicted by the root locus results, the linearized equations were also mechanized on the analog computer. Suspected coupling terms were then either disconnected or modified and the effects noted both on the root locus plots and on the analog time-histories. This experimentation indicated that the primary coupling loop was an aerodynamic-kinematic one involving angle of attack and roll rate and may be visualized with the aid of Fig. 4.

The longitudinal response is caused by the kinematic relationship between roll rate and angle of attack. From the linearized equations, the transfer function is found to be

$$\alpha/p = \tan\beta_0 \cos\alpha_0[(Mq - \lambda)/\Delta_{\text{long}}] \quad (6)$$

Similarly, the lateral-directional transfer function defining the roll rate response to angle of attack may be obtained as

$$p/\alpha = L_\alpha \{[\lambda^3 - (Y_\beta + N_r)\lambda^2 + (Y_\beta N_r + N_\beta \cos\alpha_0)\lambda - (g/V_0)N_\beta \cos\beta_0 \sin\alpha_0]/\Delta_{\text{lat}}\} \quad (7)$$

Equation (7) is simplified in that only the contribution of L_α is considered. This is because this term, which describes the influence of angle of attack on the dihedral effect, was found to be dominant over the other terms. It should be noted that L_α contains β_0 as a factor. With this in mind, it is clear that the particular form of coupling which was apparent depends upon both a nonzero equilibrium sideslip angle, and a variation of dihedral effect with angle of attack. The latter requirement is particularly well satisfied by swept-wing aircraft at moderate angles of attack.

Following the linear analysis, a brief re-examination of the coupling phenomenon was performed with the original nonlinear analog simulation of the swept-wing transport. As noted previously, and as explained by the linear analysis,

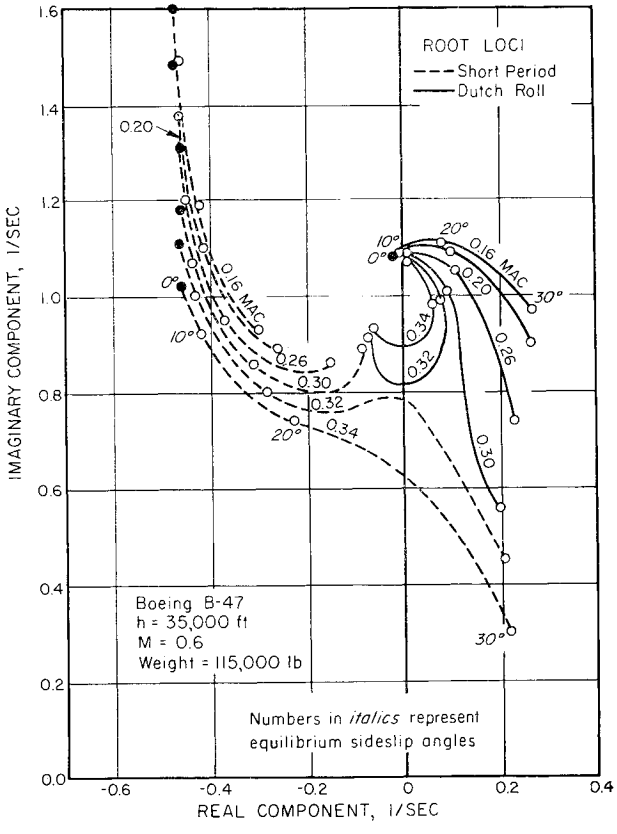

Fig. 3 Variation of short period and dutch roll roots with equilibrium sideslip angle, at a Mach number of 0.6 and various c.g. positions.

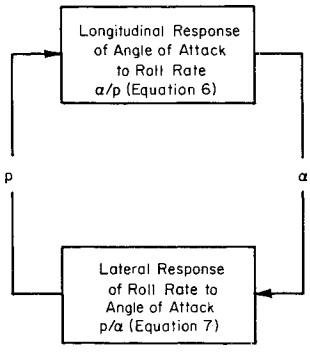

Fig. 4 Diagram illustrating closed-loop coupling between longitudinal and lateral-directional modes.

small disturbances imposed on some equilibrium sideslip flight conditions resulted in divergent motion. However, as shown in Fig. 5, the resulting motion eventually settled at a limit cycle beyond which further divergence did not occur. The linear analysis provides an explanation for this, since an examination of the slope of $C_{l\beta}$ vs angle of attack indicates that this slope vanishes at some particular angle of attack, as shown in Fig. 6. When this angle of attack is attained by an oscillation, the "gain" of the primary coupling loop goes to zero, preventing further divergence.

Conclusions

This analysis has established that significant coupling can occur between the longitudinal and lateral-directional modes if the dihedral effect is strongly dependent upon angle of attack, and if a nonzero equilibrium angle of sideslip exists. Swept-wing aircraft, by virtue of their dihedral effect characteristics, would seem to be particularly susceptible to this phenomenon; however, this study indicates that the equi-

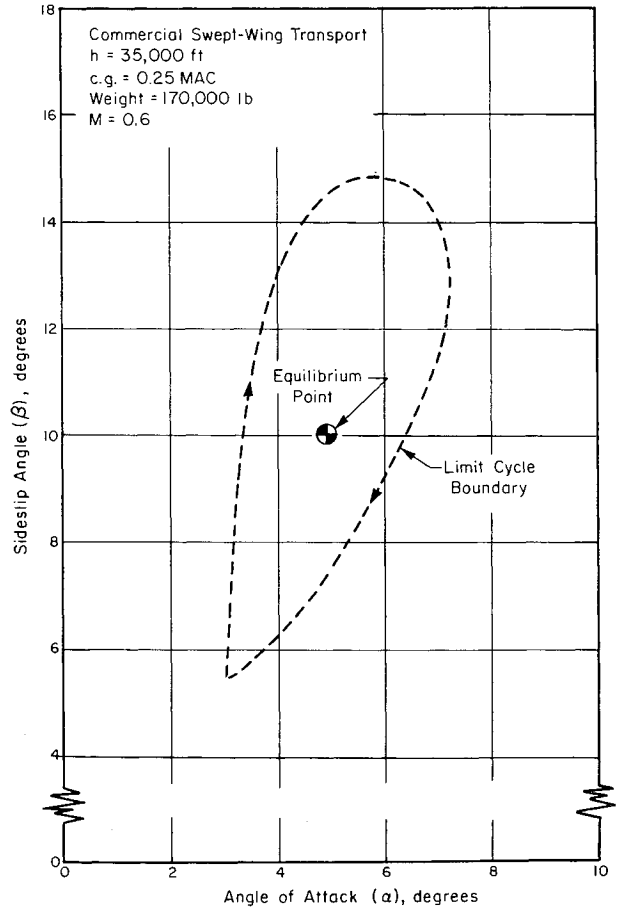

Fig. 5 Illustration of a typical limit cycle for coupled motion.

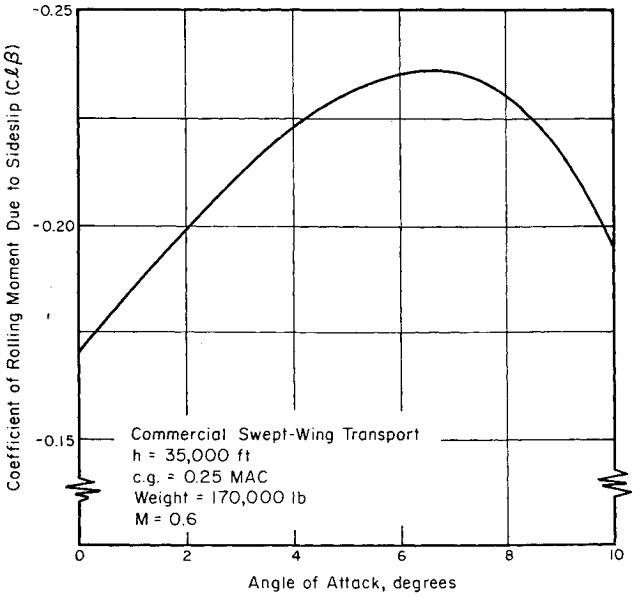

Fig. 6 Typical variation of dihedral effect with angle of attack.

librium sideslip angles required for pronounced coupling are well beyond the normal operating envelope of the class of large swept-wing aircraft which was studied.

Although it has not been established, it is possible that this phenomenon may be of some operational significance for other classes of aircraft, particularly those that may be flown with sustained sideslip, i.e., during a cross-wind landing approach.

References

[1] Etkin, B., *Dynamics of Flight* (John Wiley and Sons, Inc., New York, 1959), Chap. 4, p. 116.

[2] Cole, H. A., Jr., Brown, S. C., and Holleman, E. C., "Experimental and predicted longitudinal and lateral-directional response characteristics of a large flexible 35 degree swept-wing airplane at an altitude of 35,000 feet," NACA Rept. 1330 (1957).

Solution of an Integral Occurring in Propeller Theory

WILLIAM A. MIDDLETON*
U. S. Naval Ordnance Test Station, Pasadena, Calif.

THE integral to be solved arises in the design of propellers and in the consideration of second-order effects in subsonic airfoil theory.[1]

The integral in propeller theory is found in the form

$$M_p = \int_0^\pi \frac{\sin p\,\theta}{\cos\theta - \cos\phi}\,d\theta \tag{1}$$

where p is an integer and $0 < \phi < \pi$.

Equation (1) satisfies the recursion formula

$$M_p = [(2/p - 1)][1 - \cos(p - 1)\pi] + 2M_{p-1}\cos\phi - M_{p-2} \tag{2}$$

where $p \geq 2$ and

$$M_0 = 0 \qquad M_1 = \ln(1 - \cos\phi) - \ln(1 + \cos\phi) \tag{3}$$

A closed solution will be derived for an arbitrary integer p. The positive case is considered without loss of generality.

Iteration of the recurrence relation, Eq. (2), using the conditions stated by Eq. (3) gives, for $2 \leq p \leq k$,

$$M_p = M_1\frac{\sin p\,\phi}{\sin\phi} + 2\sum_{j=2}^{p}\frac{[1 - \cos(j-1)\pi]}{(j-1)\sin\phi} \times \sin(p - j + 1)\phi \tag{4}$$

Consider $p = k + 1$. Substituting Eq. (4) into Eq. (2) yields

$$\left.\begin{aligned} M_{k+1} &= (2/k)(1 - \cos k\pi) + 2M_k\cos\phi - M_{k-1} \\ &= \frac{2}{k}(1 - \cos k\pi) + M_1\frac{\sin(k+1)\phi}{\sin\phi} + \\ &\quad 2\sum_{j=2}^{k}\frac{[1 - \cos(j-1]\pi}{(j-1)\sin\phi}\sin(k - j + 2)\phi \end{aligned}\right\} \tag{5}$$

where use has been made of

$$\sum_{=2}^{q}\frac{[1 - \cos(j-1)\pi]}{(j-1)\sin\phi}\sin(q - j + 1)\phi = \sum_{j=2}^{q+1}\frac{[1 - \cos(j-1]\pi}{(j-1)\sin\phi}\sin(q - j + 1)\phi$$

and

$$\sin(k + 1)\phi - \sin(k - 1)\,\phi = 2\cos\phi\,\sin k\phi$$

The quantity q is an arbitrary integer greater than or equal to 2. Now

$$\frac{2}{k}(1 - \cos k\pi) + 2\sum_{j=2}^{k}\frac{[1 - \cos(j-1)\pi]}{(j-1)\sin\phi} \times \sin(k - j + 2)\phi = 2\sum_{j=2}^{k+1}\frac{[1 - \cos(j-1]\pi}{(j-1)\sin\phi} \times \sin(k - j + 2)\phi \tag{6}$$

Substituting Eq. (6) into Eq. (5) yields

$$M_{k+1} = M_1\frac{\sin(k+1)\phi}{\sin\phi} + 2\sum_{j=2}^{k+1}\frac{[1 - \cos(j-1)\pi]}{(j-1)\sin\phi} \times \sin(k - j + 2)\phi \tag{7}$$

Equation (7) is the same form as Eq. (4). Thus, if Eq. (4) is the solution to Eq. (2) for $p = k$, it is also the solution for $p = k + 1$. By the principle of mathematical induction on k, Eq. (4) is the solution to Eq. (2) for all of the integral $p \geq 2$.

Thus it follows that

$$M_p = \int_0^\pi \frac{\sin p\theta}{\cos\theta - \cos\phi}\,d\theta = M_1\frac{\sin p\phi}{\sin\phi} + 2\sum_{j=2}^{p}\frac{[1 - \cos(j-1)\pi]}{(j-1)\sin\phi} \times \sin(p - j + 1)\phi$$

for integral $p \geq 2$ and

$$M_0 = 0 \qquad M_1 = \ln[(1 - \cos\phi)/(1 + \cos\phi)]$$

Reference

[1] Van Dyke, M. D., "Second-order subsonic airfoil theory including edge effects," NACA Rept. 1274 (1956).

Received April 27, 1965; revision received July 14, 1965.
* Mathematician, Propulsion Division.